ЖЭТФ, 2014, том 146, вып. 6 (12), стр. 1192–1209

ANDREEV–MAJORANA BOUND STATES IN SUPERFLUIDS

M. A. Silaev[a,b*]***, G. E. Volovik***[a,c**]

[a] *Low Temperature Laboratory, Aalto University, P. O. Box 15100, FI-00076 Aalto, Finland*

[b] *Institute for Physics of Microstructures, Russian Academy of Sciences 603950, Nizhny Novgorod, Russia*

[c] *Landau Institute for Theoretical Physics, Russian Academy of Sciences 142432, Chernogolovka, Moscow Region, Russia*

Received May 5, 2014

We consider Andreev–Majorana (AM) bound states with zero energy on surfaces, interfaces, and vortices in different phases of the p-wave superfluids. We discuss the chiral superfluid ^{3}He-A and time reversal invariant phases: superfluid ^{3}He-B, planar and polar phases. The AM zero modes are determined by topology in the bulk and disappear at the quantum phase transition from the topological to nontopological state of the superfluid. The topology demonstrates the interplay of dimensions. In particular, the zero-dimensional Weyl points in chiral superfluids (the Berry phase monopoles in momentum space) give rise to the one-dimensional Fermi arc of AM bound states on the surface and to the one-dimensional flat band of AM modes in the vortex core. The one-dimensional nodal line in the polar phase produces a two-dimensional flat band of AM modes on the surface. The interplay of dimensions also connects the AM states in superfluids with different dimensions. For example, the topological properties of the spectrum of bound states in three-dimensional ^{3}He-B are connected to the properties of the spectrum in the two-dimensional planar phase (thin film).

Contribution for the JETP special issue in honor of A. F. Andreev's 75th birthday

DOI: 10.7868/S0044451014120050

1. INTRODUCTION

Majorana fermions are ubiquitous in superconductors and fermionic superfluids. The Bogoliubov–de Gennes equation for fermionic Bogoliubov–Nambu quasiparticles can be brought to a real form by a unitary transformation. This implies a linear relation between the particle and antiparticle field operators, which is the hallmark of a Majorana fermion. The fermionic statistics and Cooper pair correlations give rise to Majorana fermions, irrespective of geometry, dimensionality, symmetry, and topology [1–3]. The role of topology is to protect gapless Majorana fermions, which play a major role at low temperatures, when the gapped degrees of freedom are frozen out. For some combinations of geometry, dimensionality, and symmetry, these Majorana fermions behave as emergent massless relativistic particles. This suggests that Majorana fermions may serve as building blocks for constructing the Weyl particles of the Standard Model [4].

Here, we consider gapless Majorana fermions, which appear as Andreev bound states on the surfaces of superfluids and on topological objects in superfluids: quantized vortices, solitons, and domain walls. In all cases, the bound states are formed due to the subsequent Andreev reflections of particles and holes. The key factor for the formation of Andreev bound states on a small defect with the size of the order of the coherence length is a nontrivial phase difference of the order parameter at the opposite ends of the particle trajectory. In general, it depends on the structure of the order parameter in real and momentum space, which can be rather complicated. The possibilities for the formation of Andreev bound states are rather diverse, several of them are shown in Fig. 1. Particularly interesting is the case where Andreev bound states are topologically stable, which means that they have stable zero-energy Majorana modes that cannot be eliminated by a small perturbation of the system parameters.

*E-mail: msilaev@ipm.sci-nnov.ru
**E-mail: volovik@boojum.hut.fi

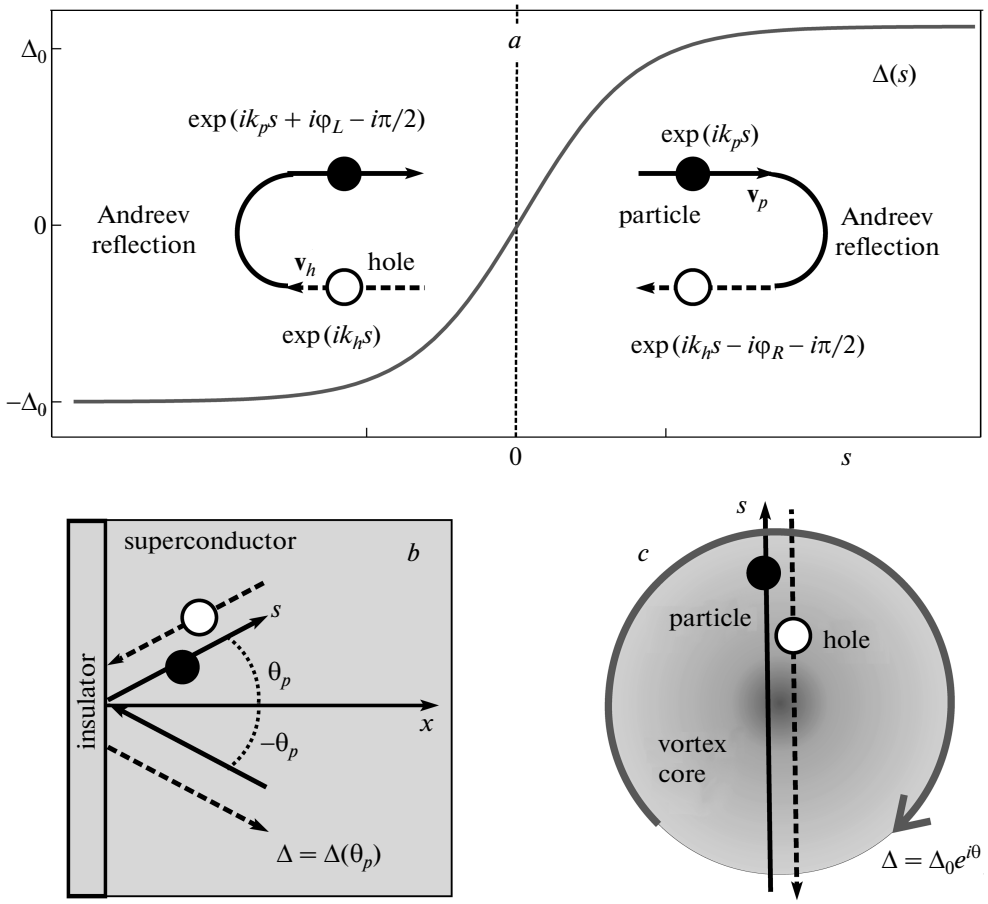

Fig. 1. Schematic picture of the formation of Andreev bound states localized (a) on domain wall, (b) on the edge, and (c) inside the vortex core. In all cases, the mechanism is the subsequent particle–hole conversions via Andreev reflections at the opposite ends of the trajectory s. The reflected particle (hole) picks up the phase of the order parameter φ_R ($-\varphi_L$) and flips the group velocity direction $\mathbf{v}_p$ ($\mathbf{v}_h$) as shown in panel a. In general, the wave vectors of the particle and the hole in the bulk are slightly different, $k_{p,h} = k_F \pm E/v_F$, where k_F and v_F are Fermi momentum and velocity, and E is the energy. If the order parameter phase difference is $\phi_R - \phi_L = \pi$, a closed loop can be formed even for $k_e = k_h$, that is, for the zero energy $E = 0$. In cases (b, c), the phase difference occurs due to the momentum dependence of the gap function and the phase winding around the vortex core correspondingly

General properties of the fermionic spectrum in condensed-matter and particle physics are determined by topology of the ground state (vacuum). The classification schemes based on topology [5–11] suggest the classes of topological insulators, fully gapped topological superfluids/superconductors, and gapless topological media. In Refs. [9–11], the classification is based on topological properties of the matrix Green's function, while other schemes explore the properties of a single-particle Hamiltonian and are therefore applicable only to systems of free (noninteracting) fermions. Among the fully gapped topological superfluids, there is time-reversal invariant superfluid ^{3}He-B, thin films of chiral superfluid ^{3}He-A, and thin films of the time-reversal invariant planar phase of superfluid ^{3}He. The main signature of topologically nontrivial vacua with the energy gap in the bulk is the existence of zero-energy edge states on the boundary, at the interface between topologically distinct domains [12, 13] and in the vortex cores [14]. For superfluids and superconductors, these are Andreev–Majorana (AM) bound states. These are mainly propagating fermionic quasiparticles, which have a relativistic spectrum at low energy [15–20]. However, for special geometries and dimensions, the AM bound state represents an isolated nonpropagating midgap state, called the Majorana zero mode (or Majorino [21]). It is not a fermion, because it obeys a non-Abelian exchange statistics [22]. This in

particular occurs for the AM bound states in the vortex core of chiral p-wave superfluid-superconductor in 2+1 dimensions [23].

A gapless AM bound state also occurs on the surfaces, interfaces, and in the vortex cores of gapless topological media. Among them, there are chiral superfluid ^{3}He-A with Weyl points, the time-reversal invariant planar phase with Dirac points, and the time-reversal invariant polar phase with a line of zeroes. The spectrum of AM bound states is nonrelativistic and exotic: the zeroes of the AM bound-state spectrum form Fermi arcs [24–27] and flat bands [28–35].

2. ANDREEV–MAJORANA EDGE STATES IN 2+1 GAPPED TOPOLOGICAL SUPERFLUIDS

The p-wave superfluid ^{3}He was discovered in 1972. But until now, there is little understanding of superfluid ^{3}He films. The information on recent experiments in confined geometry can be found in review [36]. In thin films, a competition is expected between the chiral superfluid ^{3}He-A and the time-reversal invariant planar phase, both acquiring a gap in the spectrum in the quasi-two-dimensional case due to transverse quantization.

The fermionic spectra in both the 2D A phase and the planar phase have nontrivial topological properties. These topological states provide examples of systems featuring generic topological phenomena. In particular, an analog of the integer quantum Hall effect exists in the 2D A phase, where the internal orbital momentum of Cooper pairs plays the role of the time reversal symmetry breaking magnetic field. In the time reversal invariant planar phase, the quantum spin Hall effect can be realized. In a close analogy with $2d$ electronic systems, a topological invariant is determined by the number of fermionic edge modes with zero energy. In the superfluid systems, the edge zero modes are the Andreev bound states localized at the superfluid/vacuum boundary or at the interfaces and domain walls separating superfluid states with different topological properties. Below, we discuss the topological properties and Andreev bound states for the 2D A phase and the planar phase in detail.

2.1. Chiral ^{3}He-A film

The order parameter in a spatially homogeneous time reversal symmetry breaking ^{3}He-A phase is given by

$$\hat{\Delta} = \sigma_x(p_x \pm ip_y),$$

where σ_x is the spin Pauli matrix and the $p_{x,y}$ are momentum projections onto the anisotropy plane. Such an order parameter describes spin triplet Cooper pairs with zero spin $S_z = 0$ and a nonzero oribital momentum projections $L_z = \pm 1$ onto the anisotropy axis. A nonzero L_z plays the role of the internal magnetic field breaking the time-reversal symmetry of the systems. Confined in the xy plane, the 2D state of the A phase is a fully gapped system. By the analogy with the 2D electronic gas in a quantized magnetic field, the gapped ground states (vacua) in 2+1 or quasi 2+1 thin films of ^{3}He-A are characterized by the topological invariant [37–41]

$$N = \frac{e_{ijk}}{24\pi^2} \times \\ \times \mathrm{Tr}\left[\int d^3p\, G\partial_{p_i}G^{-1}G\partial_{p_j}G^{-1}G\partial_{p_k}G^{-1}\right]. \quad (1)$$

Here, $G = G(p_x, p_y, \omega = ip_0)$ is the Green's function matrix, which depends on the Matsubara frequency p_0; the integration is over the whole (2+1)-dimensional momentum–frequency space $p_i = (p_x, p_y, p_0)$, or over the Brillouin zone and p_0 in crystals. Expression (1) is an extension of the TKNN invariant invented by Thouless, Kohomoto, Nightingale, and den Nijs to describe topological quantization of the Hall conductance [42, 43].

The advantage of the topological approach is that we can choose to work with the simplest form of the Green's function, which has the same topological properties and can be obtained from the complicated one by a continuous deformation. For a single layer of a ^{3}He-A film, we can choose

$$G^{-1} = ip_0 + \tau_3\left(\frac{p^2}{2m} - \mu\right) + c\sigma_z\left(\tau_1 p_x + \tau_2 p_y\right), \quad (2)$$

where $p^2 = p_x^2 + p_y^2$. The Pauli matrices $\tau_{1,2,3}$ and $\sigma_{x,y,z}$ respectively correspond to the Bogoliubov–Nambu spin and the ordinary spin of a ^{3}He atom; the parameter c characterizes the amplitude of the superconducting order parameter. The weak-coupling BCS limit corresponds to $mc^2 \ll \mu$. In this limit, $c = \Delta/p_F$, where Δ is the gap in the spectrum and p_F is the Fermi momentum, $p_F^2/2m = \mu$.

It is also instructive to consider the simplified case where there is only a single spin component, which corresponds to the fully spin-polarized $p_x + ip_y$ superfluid:

$$G^{-1} = ip_0 + \tau_3\left(\frac{p^2}{2m} - \mu\right) + c\left(\tau_1 p_x + \tau_2 p_y\right). \quad (3)$$

We call this case the spinless fermions. Topological invariant (1) for the state in Eq. (3) with $\mu > 0$ is $N = 1$,

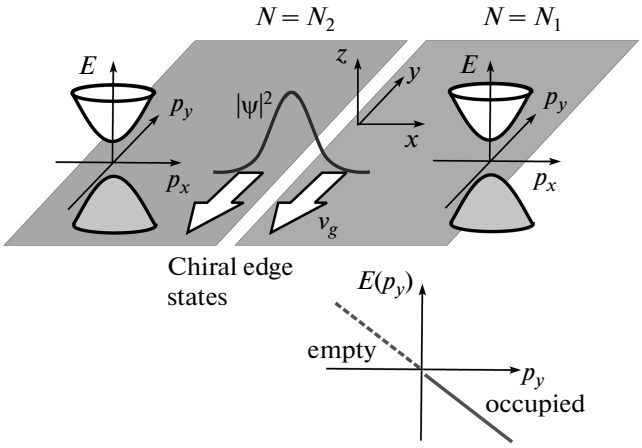

Fig. 2. Schematic picture of the interface between two films of a chiral $p_x + ip_y$ superfluid with values N_1 and N_2 of topological invariant (1). The interface contains chiral AMBSs with the spectrum $E = E(p_y)$, which move with the group velocity $v_g = dE(p_y)/dp_y$. In general, the algebraic sum of branches (the number of left-moving minus the number of right-moving fermions) is $N_2 - N_1$. On the lower panel, the chiral branch of spinless AMBSs is given by Eq. (3) with $N_2 = 1$ and $N_1 = 0$. For the spinful case in Eq. (2), there are two anomalous branches of the spectrum of edge states $E(p_y)$, which are degenerate with respect to spin. The chiral branches produce an equilibrium mass current flowing along the interface

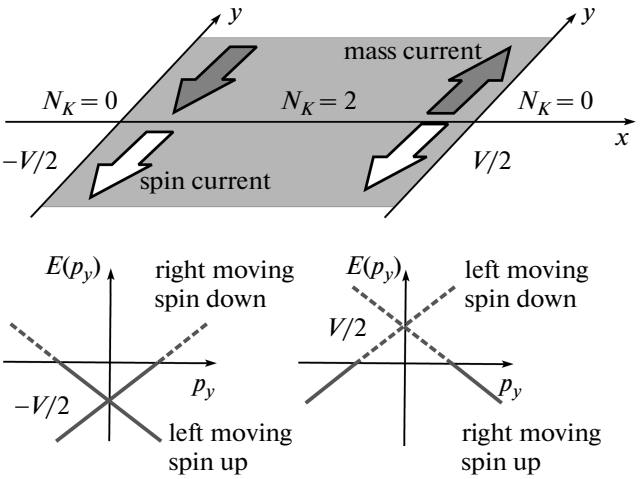

Fig. 3. An illustration of the intrinsic spin–current quantum Hall effect due to AM edge states in the stripe of a planar phase film with the topological invariant $N_K = 2$ in Eq. (6). As distinct from ^{3}He-A in Fig. 2, the anomalous branches with different spin projections have opposite slopes. This gives rise to the quantized spin Hall effect without a magnetic field, instead of the quantized Hall effect in ^{3}He-A film [41, 50]

while for the state with $\mu < 0$, we have $N = 0$. According to the bulk–surface correspondence, there must be a branch of the AM edge states at the interface between these two phases, which crosses zero energy level [15, 44] (Fig. 2).

In the spin case in Eq. (2), both spin components contribute to the topological invariant equally, and we have $N = 2$ for $\mu > 0$ and $N = 0$ for $\mu < 0$. Therefore, there must be two branches of AM edge states, which cross zero energy level. In the general case, the algebraic sum of anomalous branches (the number of left-moving minus the number of right-moving fermions) satisfies the index theorem, $n_L - n_R = N(x > 0) - N(x < 0)$.

2.2. Time-reversal invariant planar phase

In addition to the 2D chiral A phase in thin films of superfluid ^{3}He, the time-reversal invariant planar phase [45] can become stable. While this phase has not yet been identified experimentally, a strong suppression of the transverse gap in ^{3}He-B has been observed in recent experiments [36, 46–49].

The order parameter that describes the spatially homogeneous time reversal invariant planar phase has the form $\hat{\Delta} = p_y + i\sigma_z p_x$. In this phase, the order parameter is anisotropic and vanishes for the $\mathbf{p} \parallel \mathbf{e}_z$ direction, transverse to the film. Nevertheless, confined in 2D when $p_z = 0$, this system is gapful.

Being time-reversal invariant, the planar phase has a zero topological invariant of the type given by Eq. (1). But it has an extra discrete symmetry, namely, a combination of a π spin rotation around the z axis followed by a $\pi/2$ phase rotation. This modifies the topological classification, adding an extra $\mathbb{Z}$ topological invariant obtained by Volovik and Yakovenko in Ref. [41]. This invariant gives rise to the intrinsic spin Hall effect illustrated in Fig. 3.

An extra motivation to study this particular case of the planar phase is that it can be considered a cornerstone of the dimensional reduction scheme that can be applied to general class-DIII topological superconductors. In the next section, we show that the topological properties of a 3D system and an embedded (2+1)D system, which exists in any time-reversal invariant cross section of the momentum space, are connected. As an application of such a reduction, we derive a generalized index theorem for 3D topological super-

conductors, which provides an example of the bulk–boundary correspondence in odd spatial dimensions.

In the single-layer case, the simplest expression for the planar phase Green's function $G(p_0, p_x, p_y)$ is

$$G^{-1} = ip_0 + \tau_3 \left(\frac{p^2}{2m} - \mu \right) + c\tau_1(\sigma_x p_x + \sigma_y p_y). \quad (4)$$

This phase is symmetric under time reversal. The two spin components have opposite chiralities, as can be seen from the identity

$$\sigma_x p_x + \sigma_y p_y = \frac{1}{2}(\sigma_x + i\sigma_y)(p_x - ip_y) + \\ + \frac{1}{2}(\sigma_x - i\sigma_y)(p_x + ip_y). \quad (5)$$

That is why the contributions of the two spin components to topological invariant (1) cancel each other, $N = 0$. But the planar phase is still topologically nontrivial because of the discrete Z_2 symmetry between the two spin components in Eq. (5). Due to this symmetry, the matrix $K = \tau_3\sigma_z$ commutes with the Green's function, which allows introducing the symmetry-protected topological invariant [41, 50]

$$N_K = \frac{e_{ijk}}{24\pi^2} \times \\ \times \mathrm{Tr} \left[K \int d^3p\, G\partial_{p_i} G^{-1} G\partial_{p_j} G^{-1} G\partial_{p_k} G^{-1} \right]. \quad (6)$$

This invariant is robust to deformations, if the deformations are K-symmetric. For state (4) with $\mu > 0$, we have $N_K = 2$. For the general case of a quasi 2D film with multiple layers of the planar phase, the invariant N_K belongs to the group $\mathbb{Z}$. The magnetic solid-state analog of the planar phase is the 2D time reversal invariant topological insulator, which experiences the quantum spin Hall effect without an external magnetic field [12].

Figure 3 demonstrates AM edge states on two boundaries of the stripe of a single layer of a planar phase film. As distinct from ^{3}He-A in Fig. 2, the anomalous branches with different spin projections are not degenerate: they have opposite slopes, which corresponds to the zero value of the invariant $N = 0$ in Eq. (1). In the case of a superconductor with planar phase symmetry, the invariant N_K determines quantization of the spin Hall effect. In an applied voltage V, the spectra on two boundaries shift in opposite directions, changing the population of branches. This produces an imbalance in the spin currents carried by edge states on two boundaries, giving rise to a nonzero total spin current J_x^z (the current of the z-projection of spin along the x axis). This underlies the quantized spin Hall effect in the absence of a magnetic field [41, 50, 51]:

$$J_x^z = \sigma_{xy}^{spin} E_y, \quad \sigma_{xy}^{spin} = \frac{N_K}{4\pi}. \quad (7)$$

In this time reversal invariant system, the electric current quantum Hall effect is absent. The topological charge N in Eq. (1), which determines quantization of the Hall conductance in the absence of a magnetic field [40], is $N = 0$, and the currents of different spin populations cancel each other.

The mass and spin currents carried by an AM edge state in p-wave superfluids have been considered in Refs. [52, 53].

3. AM BOUND STATES ON THE SURFACE OF A 3+1 GAPPED TOPOLOGICAL SUPERFLUID

Fully gapped $3+1$ fermionic systems — topological insulators and topological superconductors — are now under extensive investigation. The interest in such systems was revived after the identification of topological insulators in several compounds [12].

These systems are characterized by gapless fermionic states on the boundary of the bulk insulator or at the interface between different states of the insulator. Historically, the topological insulators with fermionic zero modes at the interface were introduced in [54]. An example of fully gapped topological superfluids is the B phase of superfluid ^{3}He. Much attention has been devoted to the investigation of bound fermion states on the surface of ^{3}He-B. The presence of AM surface states in ^{3}He-B can be probed through anomalous transverse sound attenuation [55–58] and surface specific heat measurements [59, 60]. These AM bound states are supported by the nonzero value of the topological invariant in ^{3}He-B [20] and have a two-dimensional relativistic massless Dirac spectrum [16–19, 24].

3.1. ^{3}He-B edge states from bulk topology

A topological superfluid/superconductor of the ^{3}He-B type is described by the topological invariant N_K, which is protected by symmetry:

$$N_K = \frac{e_{ijk}}{24\pi^2} \times \\ \times \mathrm{Tr} \left[K \int d^3p\, H^{-1}\partial_{p_i} H H^{-1}\partial_{p_j} H H^{-1}\partial_{p_k} H \right]. \quad (8)$$

Here, $H(\mathbf{p})$ is the Hamiltonian, or in the case of an interacting system, the inverse Green's function at zero frequency $H(\mathbf{p}) = G^{-1}(\omega = 0, \mathbf{p})$, and K is a matrix that commutes or anticommutes with $H(\mathbf{p})$.

The proper model Hamiltonian that has the same topological properties as superfluids/superconductors of the ^{3}He-B class is the following:

$$H = \left(\frac{p^2}{2m} - \mu\right)\tau_3 - c\tau_1\boldsymbol{\sigma}\cdot\mathbf{p}, \tag{9}$$

where τ_i and σ_i are again the respective Pauli matrices of the Bogolyubov–Nambu spin and the nuclear spin. The symmetry K, which enters the topological invariant N_K in Eq. (8), is represented by the τ_2 matrix, which anticommutes with the Hamiltonian: it is the combination of time reversal and particle–hole symmetries of ^{3}He-B. In the limit $1/m = 0$, Eq. (9) transforms to the Dirac Hamiltonian, where the parameter c serves as the speed of light, while ^{3}He-B lives in the opposite limit $mc^2 \ll \mu$. The topological phase diagram in the plane $(\mu, 1/m)$ is shown in Fig. 4.

The mechanism of the Andreev–Majorana bound state formation at the edge of ^{3}He-B is clear from Hamiltonian (9). We consider the boundary plane at $x = 0$ as shown schematically in Fig. 5. Then under normal reflection of particles and holes from the boundary, some components of the gap function in Hamiltonian (9) change sign. Therefore, we obtain a nonzero phase of the gap along the effective trajectory, as shown in Fig. 1. In particular, for the trajectories normal to the boundary $p_{z,y} = 0$, the overall gap function changes sign, leading to the formation of a zero-energy state localized at the boundary.

However, this is not the whole story. Indeed, if we formally assume that the Hamiltonian may have either negative effective mass $m < 0$ or a negative chemical potential $\mu < 0$, the exact solution of the spectral problem yields no zero-energy states, as is discussed below. The hint to the topological origin of the AM bound states in ^{3}He-B can be obtained from the topological phase diagram in Fig. 4, which demonstrates that the system undergoes a topological quantum phase transitions (QPTs) as we change the sign of the chemical potential μ or the effective mass m.

The domain wall that separates the states with different values of N_K should contain the zero-energy states — the AM zero modes.

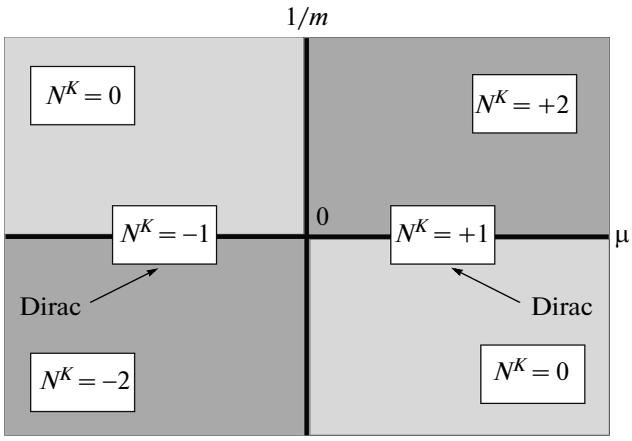

Fig. 4. Phase diagram of topological states of a triplet superfluid of the ^{3}He-B type in Eq. (9) in the plane $(\mu, 1/m)$. States on the line $1/m = 0$ correspond to the Dirac vacua, whose Hamiltonian is noncompact. The topological charge of Dirac fermions is intermediate between charges of compact ^{3}He-B states. The line $\mu = 0$ marks a topological QPT, which occurs between the weakly coupled ^{3}He-B (with $\mu > 0$, $m > 0$, and the topological charge $N_K = 2$) and the strong coupled ^{3}He-B (with $\mu < 0$, $m > 0$, and $N_K = 0$). This transition is topologically equivalent to the QPT between Dirac vacua with opposite mass parameters $M = \pm|\mu|$. The gap in the spectrum vanishes at this transition. The line $1/m = 0$ separates the states with different asymptotic behavior of the Hamiltonian at infinity: $H(\mathbf{p}) \to \pm\tau_3 p^2/2m$. The transition across this line occurs without closing the gap

3.2. ^{3}He-B edge states from topology of the planar phase

To prove the existence of the AM bound states on the surface of ^{3}He-B or at the interface, we can use a dimensional reduction. We assume that the boundary plane is at $x = 0$, and hence the conserved longitudinal momentum projections are $p_{z,y}$. To find the complete spectrum of bound states $E_b = E_b(p_y, p_z)$, it is enough to consider a set of 2D spectral problems for the cross sections of the momentum space,

$$p_y \cos\theta + p_z \sin\theta = 0, \tag{10}$$

where $2\pi > \theta \geq 0$.

An example of such a dimensional reduction to the plane $p_z = 0$ is shown in Fig. 5. The $2+1$ Hamiltonian in this cross section reduced from the 3+1 phase exactly coincides with the Hamiltonian of the planar phase. Therefore, it is classified by the integer-valued topological invariant N_K in Eq. (6), which can be shown

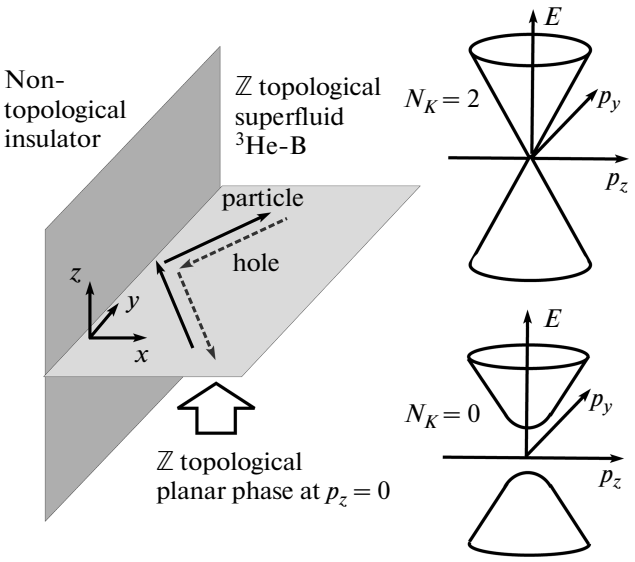

Fig. 5. Dimensional reduction of the surface-state spectral problem in 3D to that in the time-reversal invariant cross section of momentum space $p_z = 0$. Reduction from the ℤ topological superfluid ^{3}He-B results in the ℤ topological planar phase at $p_z = 0$

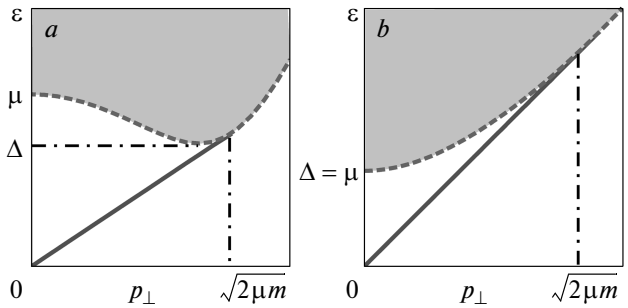

Fig. 6. Spectrum of AM fermions, localized states on the surface of a topological superfluid/superconductor of the ^{3}He-B class (solid lines) for (a) $\mu > m > 0$ and (b) $m > \mu$. The spectrum of bound states terminates when it merges with the continuous spectrum in the bulk (gray region), whose border is shown by a dashed line. The AM bound states exist for $p_\perp^2 < 2m\mu$

to coincide with the topological invariant N_K of the parent 3D ^{3}He-B phase in Eq. (8). The topologically protected AM states in ^{3}He-B are thus related to the topologically protected edge states in the $2+1$ planar phase (see details in Ref. [61]).

3.3. Evolution of the edge state at a nontopological quantum phase transition

We consider the spectrum of AM fermions using the simplest model of the interface between the superfluid and the vacuum, in which Hamiltonian (9) changes abruptly at the boundary, with the boundary condition $\psi(z = 0) = 0$.

At low energies $|E| \ll \Delta$, their spectrum is a helical spectrum, being described by the Hamiltonian $H_{AM} = c(\sigma_y p_x - \sigma_x p_y)$ [16]. Interestingly an exact solution of the spectral problem demonstrates [62] that the linear spectrum of AM bound states exist up to the merging point with the continuous spectrum of delocalized states.

For $m > 0$, the exact spectrum of AM fermions $E = \pm p_\perp$ is shown by the solid line in Fig. 6 for $E > 0$. The bound states are confined to the region $|p_\perp| < \sqrt{2m\mu}$. They disappear when their spectrum merges with the continuous spectrum in bulk. The edge of the continuous spectrum is shown by the dashed line in Fig. 6. If $mc^2 > \mu$, the minimum of the bulk energy spectrum increases monotonically with the momentum $p_\perp$, and therefore the bulk gap is

$$\Delta = \mu, \quad mc^2 > \mu. \tag{11}$$

If $\mu > mc^2$, the minimum of the bulk energy is a nonmonotonic function of $p_\perp$, having a minimum at $p_\perp^{min} = \sqrt{2m(\mu - mc^2)}$, where the bulk gap is

$$\Delta = \sqrt{mc^2(2\mu - mc^2)}, \quad 0 < mc^2 < \mu. \tag{12}$$

The line $mc^2 = \mu$ marks the nontopological QPT — a momentum-space analog of the Higgs transition [10], when the Mexican hat potential as a function of $p_\perp$ emerges for $\mu > mc^2$.

3.4. Evolution of the edge state at a topological quantum phase transition

We first consider the behavior of the spectrum of Majorana fermions at the topological transition at which m crosses zero. As m approaches zero, $m \to 0$, the region of momenta where bound states exist shrinks and finally, for $m < 0$, i. e., in the topologically trivial superfluid, no bound states exist any more. Simultaneously the gap in the bulk, which at small m is $\Delta \approx \sqrt{2mc^2\mu}$ according to Eq. (12), decreases with decreasing m and vanishes at $m = 0$. This corresponds to the conventional scenario of a topological QPT, when at the phase boundary between the two gapped states with different topological numbers, the gap is closed.

The same happens at the topological QPT occurring when μ crosses zero (see the phase diagram in Fig. 4).

We now consider what happens with bound states in the case where the topological QPT occurs in the opposite limit, when m changes sign via infinity, i. e., when $1/m$ crosses zero. This topological transition occurs without closing the gap. In this case, the bound states formally exist for all p_x even in the limit $1/m \to 0$. But in this limit, the ultraviolet divergence occurs: the characteristic length scale of the wave function of the bound state $L \propto \hbar/mc \to 0$. Hence, if the topological QPT from a topologically nontrivial to the trivial insulator (or superconductor) occurs without closing the gap, the gapless spectrum of surface states disappears by escaping via the ultraviolet. This limit corresponds to the formation of a zero of the Green's function, $G = 1/(i\omega - H) \to 0$. Such a scenario is impossible in the models with a bounded Hamiltonian [63, 64], as in the approximation of a finite number of crystal bands.

On the other hand, the Green's function zeroes can occur due to particle interactions. As was found in Ref. [65], classifications of interacting and noninteracting fermionic systems do not necessarily coincide. This is related to zeroes of the Green's function, which according to Ref. [10] contribute to topology alongside with the poles. Due to zeroes, the integer topological charge of an interacting system can change without closing the energy gap, and it is suggested that this may lead to the occurrence of topological insulators with no fermion zero modes on the interface [63, 64].

That is why we expect that the same scenario with an escape to the ultraviolet occurs for interacting systems: if due to zeros in the Green's function, the topological QPT in the bulk occurs without closing the gap, the spectrum of edge states does nevertheless change at the topological QPT, and this change occurs via the ultraviolet.

We finally mention that the magnetic field violates time reversal symmetry, which generically leads to a finite gap (mass) in the spectrum of AM fermions on the surface. At a particular orientation of the magnetic field, there is still the Z_2 dsicrete symmetry, which supports gapless AM bound states [66, 67]. This symmetry is spontaneously broken at some critical value of the magnetic feild, above which the AM fermions become massive. The surface of ^{3}He-B with massive AM bound states represents a $2+1$ topological "insulator": it is described by the topological invariant in Eq. (1). The line on the surface that separates the surface domains with different values of this topological invariant contains $1+1$ gapless AM fermions [68].

4. ANDREEV–MAJORANA BOUND STATES ON THE SURFACE OF A 3+1 WEYL SUPERFLUID. FERMI ARC

We now move to the AM bound states that appear as edge and vortex states in gapless topological systems. Here, the zeroes in the bulk lead to extended zeroes on the surfaces, interfaces, and vortex cores. We start with point zeroes — Weyl points — in chiral superfluids, which produce the lines of zeroes (Fermi arcs) on the surface, and the flat band in the vortex core.

4.1. Andreev–Majorana Fermi arc on the boundary of a Weyl superfluid

The topological origin of AM bound states in $3+1$ chiral superfluids can be viewed by extending the topology of the $2+1$ chiral system in Sec. 2 to the $3+1$ case. For simplicity, we consider spinless fermions, or, which is the same, the fermions with a given spin polarization. Then the Green's function in Eq. (2) extended to the $3+1$ case is

$$G^{-1}(\mathbf{p}, p_0) = ip_0 + \tau_3 \left(\frac{p^2}{2m} - \mu \right) + \\ + c\left(\tau_1 p_x + \tau_2 p_y\right), \quad (13)$$

where $\mathbf{p} = (p_x, p_y, p_z)$. We regard p_z as a parameter of the $2+1$ system. Then for each p_z, except $p_z = \pm p_F$, this Green's function describes the fully gapped $2+1$ system — an "insulator" characterized by the topological invariant in Eq. (1):

$$N(p_z) = \frac{1}{4\pi^2} \operatorname{Tr} \left[\int dp_x dp_y dp_0 \times \right. \\ \left. \times G\partial_{p_x} G^{-1} G \partial_{p_y} G^{-1} G \partial_{p_0} G^{-1} \right]. \quad (14)$$

This insulator is topological for $|p_z| < p_F$, where $N(|p_z| < p_F) = 1$, and is topologically trivial for $|p_z| > p_F$, where $N(|p_z| > p_F) = 0$.

At $p_z = \pm p_F$, invariant (14) is not determined, since the corresponding $2+1$ system is gapless. The bulk $3+1$ superfluid ^{3}He-A has two points in the spectrum $\mathbf{p}_\pm = (0, 0, \pm p_F)$ where the energy is zero, see Fig. 7. These nodes in the spectrum are topologically protected, because they represent monopoles in the Berry phase in the momentum space and are characterized by the topological invariant in Eq. (1), where the integration is now over the 3D sphere around the Weyl point in the $3+1$ space (p_0, p_x, p_y, p_z) [9]. In the vicinity of these points, the fermionic quasiparticles behave as chiral (left-handed and right-handed) Weyl fermions

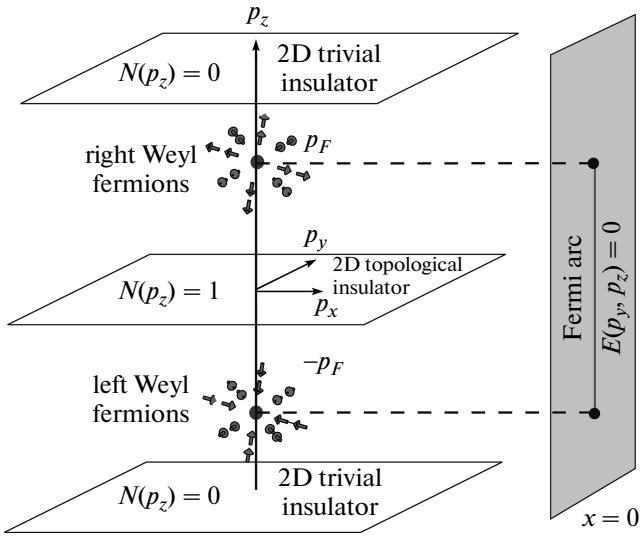

Fig. 7. Line of AM bound states on the surface of a chiral superfluid with Weyl points. This line represents a 1D Fermi surface that separates the edge states with positive and negative energies (see also Fig. 9). However, as distinct from conventional Fermi surfaces, this Fermi surface has end points. The end points of the Fermi arc are determined by projections of the bulk Weyl points to the surface

in particle physics. That is why such nodes are called the Weyl points. Arrows in Fig. 7 show the direction of the effective spin of the Weyl fermion. This spin is parallel to $\mathbf{p} - \mathbf{p}_+$ in the vicinity of $\mathbf{p}_+$, which means that the fermions living there are right-handed. For the left-handed fermions near $\mathbf{p}_-$, their effective spin is antiparallel to $\mathbf{p} - \mathbf{p}_-$.

According to the bulk–surface correspondence, at each p_z for which $N(p_z) = 1$, there should be one branch of AM edge states that crosses the zero energy level (see Fig. 2). As a result, we have a line of zero-energy states in the range $-p_F < p_z < p_F$. This line represents the Fermi surface (Fermi line) in the two-dimensional momentum space of bound states. As the conventional Fermi surface, it separates the positive- and negative-energy levels, but in contrast to the conventional Fermi surface, this Fermi surface is not closed. It has two end points, and this is why this line is called the Fermi arc.

The end points of the Fermi arc coincide with the projection of the Weyl points to the surface. This is a consequence of the bulk–surface correspondence in Weyl systems [25]. For an arbitrary direction of the surface with an angle λ between the normal to the surface and the z axis, the Fermi arc is concentrated in the range of momenta $-p_F \sin\lambda < p_z < p_F \sin\lambda$. We note that in ^{3}He-A, the boundary conditions require $\lambda = 0$.

In crystals, the Weyl points can be moved to the boundaries of the Brillouin zone, where they annihilate each other. As a result, we obtain a chiral $3+1$ topological insulator or a fully gapped chiral topological superconductor. Since $N(p_z) = 1$ for all p_z, the topological Fermi arc on the boundaries transforms to a closed topological Fermi surface.

4.2. Andreev–Majorana Fermi arcs on solitons and domain walls

Similar Fermi arcs appear on the domain walls or solitons separating the chiral phases with opposite chiralities. We have $N(|p_z| < p_F) = +1$ on one side of the soliton/wall and $N(|p_z| < p_F) = -1$ on the other side. According to the index theorem [9, 44], the difference between these two values determines the number of zero modes at the interface between the $2+1$ topological insulators for each $|p_z| < p_F$. As a result, the domain wall and the soliton contain two Fermi arcs instead of a single Fermi arc on the boundary (Fig. 8).

A Fermi arc on domain walls in ^{3}He-A [70] has been considered in Refs. [27, 71].

Figure 9 also includes bound states with a nonzero energy and demonstrates that the Fermi arc does represent a piece of the Fermi surface that separates the positive- and negative-energy levels.

5. TOPOLOGICAL SUPERFLUIDS WITH LINES OF ZEROES. THE ANDREEV–MAJORANA SURFACE FLAT BAND

The zero-dimensional point nodes in the bulk (Weyl points) give rise to one-dimensional nodes (lines) in the spectrum of AM bound states. In the same manner, the 1D nodal lines in the bulk give rise to 2D manifolds of AM bound states with zero energy (Fig. 10). We consider the topological origin of such dispersionless spectrum — a flat band — with the example of the polar phase of a triplet superfluid/superconductor [32].

5.1. Flat band of Andreev–Majorana modes on the surface of the polar phase

The Hamiltonian for the polar phase is

$$H = \left(\frac{p^2}{2m} - \mu\right)\tau_3 - c\tau_1\sigma_z p_z. \qquad (15)$$

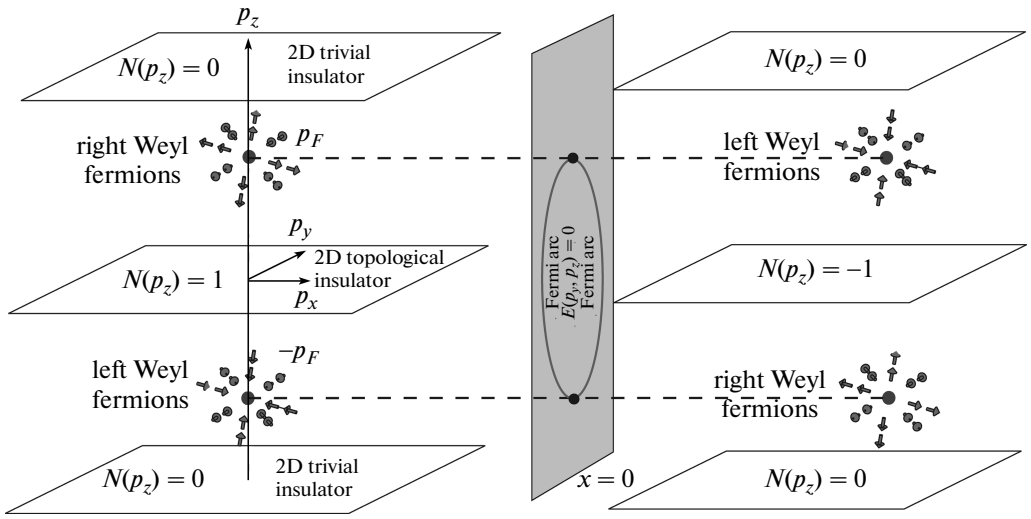

Fig. 8. Topology of Andreev bound states on a $\hat{1}$ soliton [69]. The momentum space topology of Weyl points in bulk ^{3}He-A on two sides of the soliton prescribes the existence of Fermi arcs in the spectrum of Andreev bound states in the soliton or at the interface between the bulk states with different positions of Weyl points. In the considered case, the Weyl points on two sides of the interface have the same positions in momentum space, but the opposite chiralities. As a result, the $2+1$ topological insulators have opposite topological invariants, $N(p_z = 0) = \pm 1$. This leads to two Fermi arcs terminating on the projections of the Weyl points on the soliton/interface plane in accordance with the index theorem $n(\text{right}) - n(\text{left}) = 2$

This superconductor obeys the time reversal and space inversion symmetry, and it has a line of zeroes in the form of a ring.

For simplicity, we consider spinless fermions, or, which is the same, the fully spin-polarized fermions, whose Hamiltonain is

$$H = \left(\frac{p^2}{2m} - \mu\right)\tau_3 - c\tau_1 p_z. \qquad (16)$$

The spectrum of such fermions has a nodal line — the ring $p_x^2 + p_y^2 = p_F^2$, $p_z = 0$. The stability of this nodal line is determined by the topological invariant protected by symmetry,

$$N_K = \frac{1}{4\pi i}\,\mathrm{Tr}\left[K \oint\limits_C dl\, H^{-1}\nabla_l H\right]. \qquad (17)$$

Here, the integral is along a loop C around the nodal line in the momentum space (Fig. 11), and the matrix $K = \tau_2$ anticommutes with the Hamiltonian. The winding number around the element of the nodal line is $N_K = 1$.

We now consider the momentum $\mathbf{p}_\perp$ as a parameter of the $1+1$ system; then for $|\mathbf{p}_\perp| \neq p_F$, the system represents the fully gapped state, a $1+1$ insulator. This insulator can be described by the same invariant as in Eq. (17) with the integration contour chosen parallel to p_z. Because the Hamiltonian tends to the same limit as $p_z \to \pm\infty$, the points $p_z = \pm\infty$ are equivalent, and the line $-\infty < p_z < \infty$ forms a closed loop. That is why the integral

$$N_K(\mathbf{p}_\perp) = \frac{1}{4\pi i}\,\mathrm{Tr}\left[K \int_{-\infty}^{\infty} dp_z\, H^{-1}\nabla_{p_z} H\right] \qquad (18)$$

is integer valued.

The topological invariant $N(\mathbf{p}_\perp)$ in (18) determines the properties of the surface bound states of the $1+1$ system at each $\mathbf{p}_\perp$. Due to the bulk–edge correspondence, the topological 1D insulator must have a surface state with exactly the zero energy. Because such states exist for any parameter within the circle $|\mathbf{p}_\perp| = p_F$, we obtain a flat band of AM modes in Fig. 11 *a* — the continuum of self-conjugate bound states with exactly the zero energy, $E(|\mathbf{p}_\perp| < p_F) = 0$, which are protected by topology. Such modes do not exist for parameters $|\mathbf{p}_\perp| > p_F$, for which the $1+1$ superfluid is nontopological.

In the spin polar phase with Hamiltonian (15), the nodal ring in the bulk gives rise to two surface flat bands with opposite chiralities for two directions of spin. The tiny spin–orbit interaction leads to a small splitting of the AM modes.

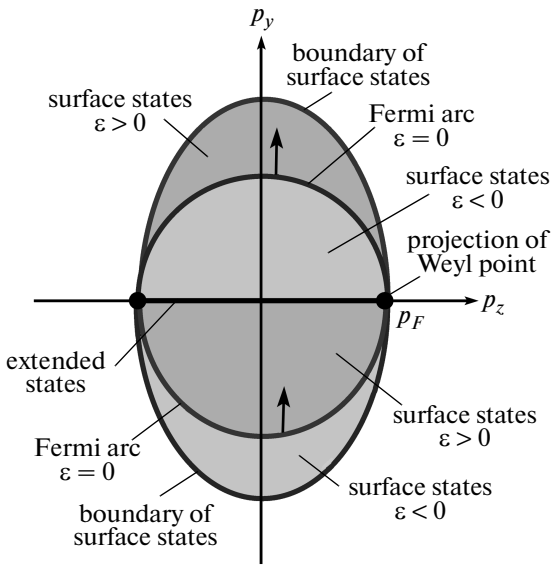

Fig. 9. The spectrum of bound states with two Fermi arcs $\varepsilon(p_y, p_z) = 0$. The arrows show directions of the Fermi velocity at these Fermi arcs. At $p_z = 0$, the velocity is in the same direction, $v_y > 0$, which demonstrates that both Fermi arcs have the same topological charge $N = +1$, which together satisfy the index theorem $n(\text{right}) - n(\text{left}) = 2$, in agreement with the momentum space topology of Weyl points in bulk ^{3}He-A on two sides of the soliton in Fig. 8. This leads to a discontinuity in the spectrum of bound states at $p_y = 0$, where the spectrum merges with the bulk spectrum

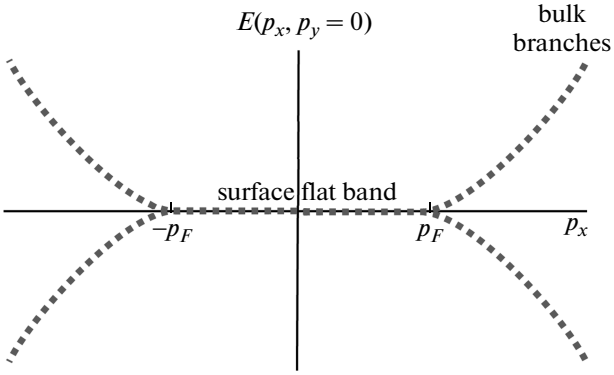

Fig. 10. Spectrum of AM modes on the surface of the polar phase. These modes form a 2D flat band: all the states with $p_x^2 + p_y^2 < p_F^2$ have zero energy. The spectrum is shown for $p_y = 0$

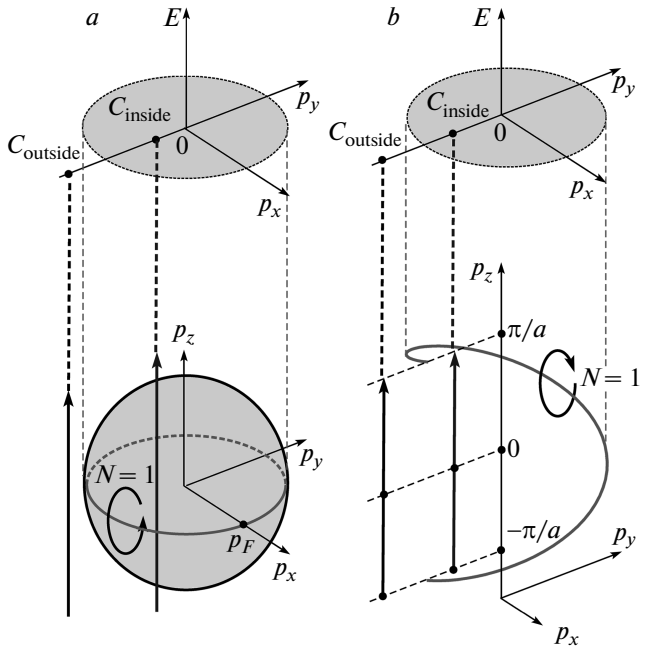

Fig. 11. Topologically nontrivial nodal lines generate topologically protected flat bands on the surface: (a) closed equatorial line of zeros in the polar phase; (b) spiral of zeros in the multilayered graphene is also a closed line. Projection of the line on the surface determines boundary of flat band. If for a fixed (p_x, p_y) the energy $E(p_x, p_y, p_z)$ is nonzero for any p_z, then the Green's function $G(\omega, p_z)_{p_x, p_y}$ describes a 1D fully gapped system, an "insulator". At each (p_x, p_y) inside the projection of the line to the surface, this insulator is topological, since it is described by nonzero topological invariant (18). Thus, for such (p_x, p_y), there is a gapless edge state on the surface. The manifold of these zero-energy edge state inside the projection forms the flat band

5.2. Flat band on the surface of model graphite

In the multilayered graphene, when the number of graphene layers tends to infinity, and if some small matrix elements are neglected, the resultant $3+1$ system has a line of zeroes, which also obeys an invariant similar to that in Eq. (17). This nodal line has the shape of a spiral [32, 33] (Fig. 11).

We again consider the momentum $\mathbf{p}_\perp$ as a parameter of the $1+1$ system; then for $|\mathbf{p}_\perp| \neq t$, where t is the dominating hopping element, the system represents the fully gapped system, a $1+1$ insulator. This insulator can be described by the same invariant as in Eq. (17) with the integration contour chosen parallel to p_z, i. e., along the 1D Brillouin zone at a fixed $\mathbf{p}_\perp$. Due to periodic boundary conditions, the points $p_z = \pm\pi/a$, where

a is the distance between the layers, are equivalent and the contours of integration form a closed loop. As a result, we obtain the integer-valued invariant

$$N_K(\mathbf{p}_\perp) = \frac{1}{4\pi i}\,\mathrm{Tr}\int_{-\pi/a}^{\pi/a} dp_z\,\tau_2 H^{-1}\nabla_{p_z} H. \qquad (19)$$

For $|\mathbf{p}_\perp| < t$, the $1+1$ insulator is topological because $N(|\mathbf{p}_\perp| < t) = 1$. This gives rise to a surface flat band. Since there are no Cooper-pair correlations, the fermionic bound states within the flat band are not Majorana modes.

6. ANDREEV–MAJORANA MODES ON VORTICES IN CHIRAL $2+1$ SUPERFLUIDS

The low-energy fermions bound to the vortex core play the main role in the thermodynamics and dynamics of the vortex state in superconductors and Fermi superfluids. The spectrum of low-energy bound states in the core of an axisymmetric vortex with the winding number $\nu = \pm 1$ was obtained by Caroli, de Gennes, and Matricon for the isotropic model of an s-wave superconductor in the weak-coupling limit $\Delta \ll \mu$ [72]:

$$E_n(p_z) = -\nu\omega_0(p_z)\left(n + \frac{1}{2}\right). \qquad (20)$$

This spectrum is two-fold degenerate due to spin degrees of freedom. The integer number n is a quantum number related to the angular momentum of the bound-state fermions. The minigap — the level spacing $\omega_0(p_z)$ — corresponds to the angular velocity of the fermionic quasiparticle orbiting the vortex axis. The direction of rotation is determined by the sign of the winding number ν of the vortex.

The level spacing is typically small compared to the energy gap of the quasiparticles outside the core, $\omega_0 \sim \Delta^2/\mu \ll \Delta$. Hence, in many physical cases, the discreteness of n can be neglected. In such cases, the spectrum crosses zero energy as a function of the continuous angular momentum L_z, and we can consider this as a spectrum of quasi zero modes. The fermions in this 1D "Fermi liquid" are chiral: the positive-energy fermions have a definite sign of the angular momentum L_z. The number of the branches crossing zero energy as a function of continuous L_z obeys the index theorem [9].

Here, we are interested in the fine structure of the spectrum, when its discrete nature is important. This takes place, for example, in ultracold fermionic gases near the Feshbach resonance, when Δ is not small.

We first consider the $2+1$ space–time and start with the weak-coupling limit. The Majorana nature of the Bogoliubov particles requires that the spectrum must be symmetric with respect to zero energy, i. e., for each level with an energy E, there must be a level with the energy $-E$. For fermions on vortices, such condition is satisfied for two classes of systems. In systems of the first class, the spectrum of Andreev bound states is $E_n = \omega_0(n+1/2)$. Vortices in s-wave superconductors belong to this class. Vortices of the second class have $E_n = \omega_0 n$. They contain an AM mode exactly with the zero energy level at $n = 0$. In a $2+1$ system, this mode is not propagating and is self-conjugate. That is why it is called the Majorana mode instead of a Majorana particle (see Ref. [21]).

For simplicity, we consider the spinless (or fully spin polarized) chiral $p_x + ip_y$ superfluid in a $2+1$ space–time, which is described by Eq. (3). As was shown in Ref. [23], the vortices with the winding number $\nu = 1$ or $\nu = -1$ belong to the second class:

$$E_n = -\nu\omega_0 n, \qquad (21)$$

and hence contain a single Majorana mode at $n = 0$. This mode is robust to perturbations, since it is self-conjugate and must therefore obey the condition $E = -E$ (see also [73]).

For the spin fermions in Eq. (2), there are two AM modes corresponding to the two spin projections. The even number of Majorana modes is not robust to perturbations. For example, the spin-orbit interaction splits two modes with $E_1 = -E_2$. The splitting is absent if there is some discrete symmetry between the AM modes, such as the mirror symmetry in Ref. [74].

In the spin $p_x + ip_y$ superfluids, there is a topological object that carries a single Majorana mode. It is the half-quantum vortex [75]. In a simple model, the half-quantum vortex is the vortex with $\nu_\uparrow = 1$ in one spin component, while the other spin component has zero vorticity $\nu_\downarrow = 0$. As a result, such vortex contains a single Majorana mode, which is robust to perturbations.

However, the perturbations should not be too large. In the limit when μ is negative and large, the BCS is transformed to the BEC of molecules, where the Majorana mode is absent. The Majorana mode disappears when the chemical potential μ crosses zero. At $\mu = 0$, there is a topological QPT, at which the topological invariant in Eq. (1) changes from $N = 1$ to $N = 0$. The topological transition cannot occur adiabatically, and in the intermediate state with $\mu = 0$, the spectrum in the bulk becomes gapless. At $\mu = 0$, the Majorana mode merges with the continuous spectrum

of bulk quasiparticles and disappears at $\mu < 0$. This demonstrates the topological origin of the AM mode, which exists inside the vortex only if the vacuum in the bulk is topologically nontrivial.

7. AN ANDREEV–MAJORANA FLAT BAND IN A VORTEX IN WEYL SUPERFLUIDS

We can easily extend the consideration in Sec. 6 to the $3+1$ case in the weak-coupling limit. The levels at $p_z \neq 0$ remain equidistant according to the Caroli–de Gennes–Matricon solution, and they must be symmetric with respect to $E = 0$. This dictates the following modification of Eq. (20) for the most symmetric vortices in ^{3}He-A and in the planar phase:

$$E_n(p_z) = -\nu\omega_0(p_z)n. \tag{22}$$

This equation suggests a flat band in the vortex core for $n = 0$ (Fig. 12a). We now show how such a flat band emerges purely from topological considerations, which do not use the weak-coupling approximation.

Topology of bound states on vortices in $3+1$ chiral superfluids can be obtained by dimensional extension of the topology in the $2+1$ case. The AM mode in a point vortex of a fully gapped $2+1$ chiral superfluid

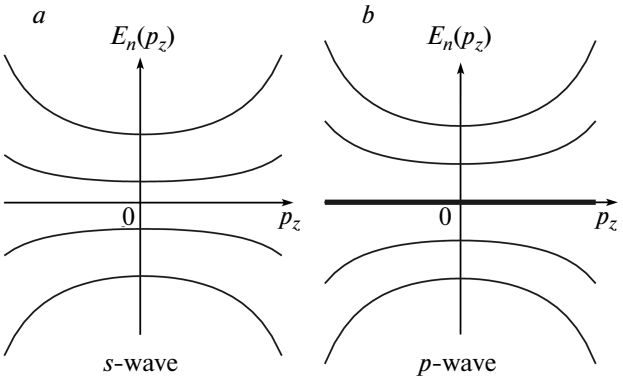

Fig. 12. (a) Schematic illustration of the spectrum of fermionic bound states in the core of a $\nu = 1$ vortex in the s-wave superconductor. In the weak-coupling limit, the lowest branches are equidistant: $E_n(p_z) = -\omega_0(p_z)(n + 1/2)$. There are no zero-energy states. The spectrum is doubly degenerate with respect to spin. (b) The spectrum of bound states in the most symmetric vortices in the p-wave superfluids: the chiral Weyl superfluid ^{3}He-A and the time reversal invariant planar phase. The spectrum is $E_n(p_z) = -\omega_0(p_z)n$. The branch with $n = 0$ forms a flat band of AM modes (solid line)

transforms into the flat band of AM modes inside the vortex line in $3+1$ chiral superfluids with Weyl points in the bulk. We consider the $p_x + ip_y$ state in Eq. (13) again, and temporarily choose the direction of the vortex line along the z axis. In this case, p_z is the quantum number of bound states in the vortex core. For each p_z in the range $-p_F < p_z < p_F$, the Green's function (13) describes the $2+1$ chiral superfluid with the topological invariant $N(|p_z| < p_F) = 1$ in Eq. (14), and this superfluid contains a point vortex. The point vortex in the $2+1$ topologically nontrivial chiral superfluid contains the AM mode with zero energy. The continuum of AM modes in the range $-p_F < p_z < p_F$ forms the flat band.

This is demonstrated in Fig. 13, where the vortex axis is rotated through an angle λ with respect to the direction to the Weyl points. In this case, invariant (14) becomes

$$N(p_z) = 1, \quad |p_z| < p_F|\cos\lambda|, \tag{23}$$

$$N(p_z) = 0, \quad |p_z| > p_F|\cos\lambda|. \tag{24}$$

Such a flat band of AM modes has been predicted by Kopnin and Salomaa in Ref. [28] for the $\nu = 1$ vortex in ^{3}He-A. This flat band is doubly degenerate with respect to spin and can therefore split, for example, due to spin–orbit interaction (the nondegenerate flat band of AM fermions occurs in the core of a half-quantum vortex). In superfluid ^{3}He, the spin–orbit interaction is very small and can be neglected. However, there can be another source of splitting: the symmetry of the vortex core can be spontaneously broken [75].

The same doubly degenerate flat band should exist in the $\nu = 1$ vortex in the $3+1$ planar phase, where the Green's function is

$$G^{-1} = ip_0 + \tau_3\left(\frac{p^2}{2m} - \mu\right) + \tau_1(\sigma_x p_x + \sigma_y p_y). \tag{25}$$

Here, $p^2 = p_x^2 + p_y^2 + p_z^2$. For the $3+1$ planar phase, the topological invariant N_K in Eq. (6) is extended to

$$N_K(p_z) = \frac{1}{4\pi^2}\,\mathrm{Tr}\left[K\int dp_x dp_y dp_0\, G\partial_{p_x} \times \right.$$
$$\left. \times\, G^{-1}G\partial_{p_y}G^{-1}G\partial_{p_0}G^{-1}\right], \tag{26}$$

giving $N_K(|p_z| < p_F\cos\lambda) = 2$.

Both flat bands, in the A-phase and in the planar phase, appear only for $\mu > 0$, when $N_K(p_z = 0) = 2$. For $\mu < 0$, the superfluids are topologically trivial, $N_K(p_z = 0) = 0$, and the flat band does not exist.

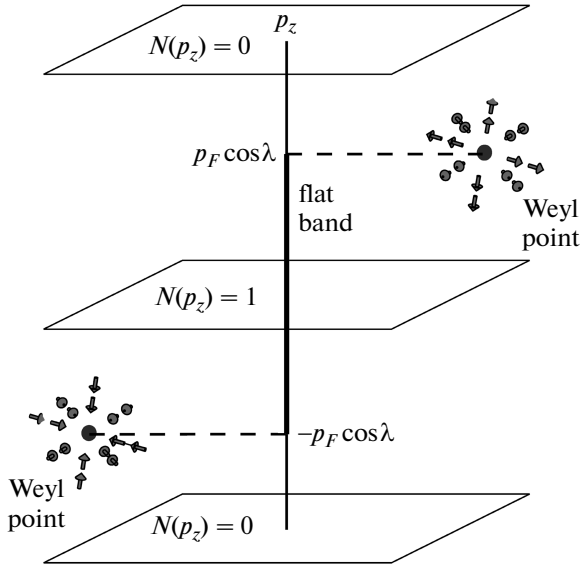

Fig. 13. Projections of Weyl points on the direction of the vortex axis (the z axis) determine the boundaries of the flat band in the vortex core. A Weyl point in a 3D system represents the hedgehog (Berry-phase monopole) in momentum space [9]. For each plane $p_z = \text{const}$, we have the effective 2D system with the fully gapped energy spectrum $E_{p_z}(p_x, p_y)$, except for the planes with $p_{z\pm} = \pm p_F \cos\lambda$, where the energy $E_{p_z}(p_x, p_y)$ has a node due to the presence of the hedgehogs. The topological invariant $N(p_z)$ in (14) is nonzero for $|p_z| < p_F|\cos\lambda|$, which means that for any value of the parameter p_z in this interval, the system behaves as a 2D topological insulator or a 2D fully gapped topological superfluid. A point vortex in such 2D superfluids has a fermionic state with exactly the zero energy. For the vortex line in the original 3D system with Fermi points, this corresponds to the dispersionless spectrum of fermion zero modes in the whole interval $|p_z| < p_F|\cos\lambda|$ (thick line). The flat band terminates at points, where the spectrum of bond states merges with the spectrum of bulk excitations (see Fig. 14)

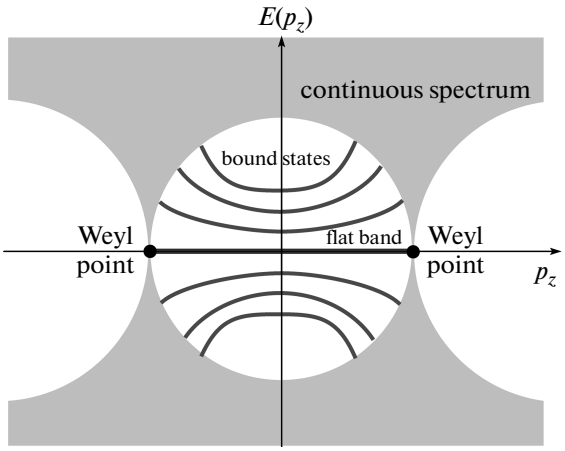

Fig. 14. Schematic illustration of the spectrum of bound states $E(p_z)$ in the vortex core of a Weyl superfluid. The branches of bound states terminate at points where their spectrum merges with the continuous spectrum in the bulk. The flat band terminates at points where the spectrum has zeros in the bulk, i. e., when it merges with Weyl points. This is a p-space analog of a Dirac string terminating on a monopole; another analog is given by the Fermi arc in Fig. 1*c*

8. ANDREEV–MAJORANA BOUND STATES IN A ^{3}He-B VORTEX

8.1. From the planar phase to the B-phase

Dimensional extension of the $2+1$ planar phase allows understanding the topological properties of the vortex spectrum in ^{3}He-B. The Hamiltonian (9) for fermions in the bulk ^{3}He-B represents the $2+1$ planar phase at $p_z = 0$. That is why at $p_z = 0$, the $\nu = 1$ vortex in ^{3}He-B contains two AM bound states with zero energy, if the tiny spin–orbit interaction is neglected and the core symmetry is not spontaneously broken. For $p_z \neq 0$, the zero-energy modes are not supported by topology. Hence, the two branches of AM modes split, and we may expect the spectrum of AM bound states in the most symmetric vortex to behave as illustrated in Fig. 15.

For ^{3}He-B, which lives in the range of parameters where $N_K \neq 0$ in Fig. 15*a*, the gapless fermions in the core of the most symmetric vortex (the so-called o-vortex [75]) were found in Ref. [76]. On the other hand, in the Bose–Einstein condensate (BEC) limit, when μ is negative and the Bose condensate of molecules occurs, there are no gapless fermions (see Fig. 15*b*). Thus, in the BCS–BEC crossover region, the spectrum of fermions localized on vortices must be reconstructed. The topological reconstruction of the fermionic spectrum in the vortex core cannot occur adiabatically. It should occur only during a topological QPT in the bulk, when the bulk gapless state is crossed. Such a topological transition occurs at $\mu = 0$ (see Fig. 4). At $\mu < 0$, the topological charge N_K vanishes and simultaneously the gap in the spectrum of core fermions arises (see Fig. 15*b*).

This again demonstrates that the existence of fermion zero modes is closely related to the topological properties of the vacuum state. The reconstruction of the spectrum of fermion zero modes at the topologi-

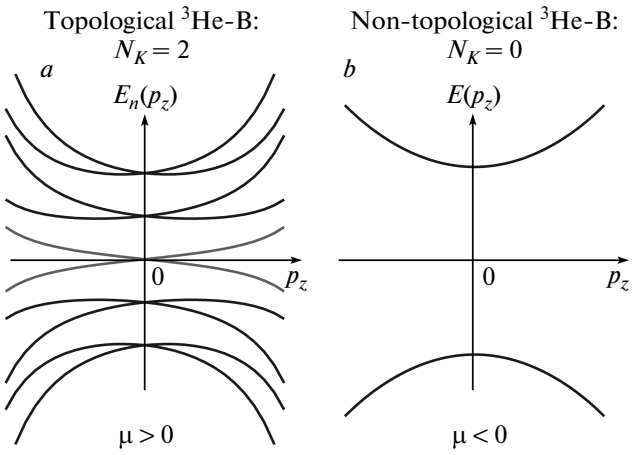

Fig. 15. (a) Schematic illustration of the spectrum of fermionic bound states in the core of the most symmetric vortex (o-vortex) in ^{3}He-B. Two AM states with zero energy exist at $p_z = 0$. (b) The same vortex but in the topologically trivial state of the liquid, $N_K = 0$, does not have fermion zero modes. The spectrum of bound states is fully gapped. Fermion zero modes disappear at the topological QPT, which occurs in bulk liquid at $\mu = 0$. A similar situation may occur for strings in color superconductors in quark matter [77]

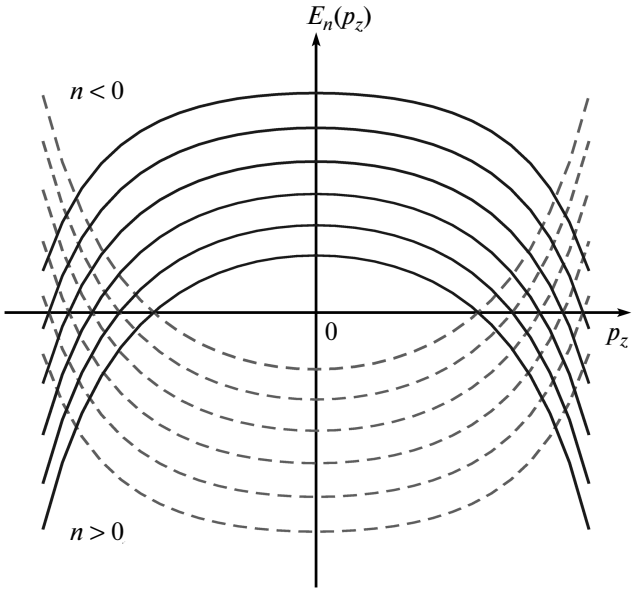

Fig. 16. Spectrum of AM bound states in an axisymmetric v-vortex with spontaneously broken discrete symmetry in ^{3}He-B. The AM states with zero energy at $p_z = 0$, which were present in the most symmetric o-vortex in Fig. 15, do not exist any more. They split due to the matrix element between the spin components, which appears due to symmetry breaking, and move far away. There are many nontopological branches of the spectrum, which cross zero energy as functions of p_z and form one-dimensional Fermi surfaces. The number of such branches is of the order of $\sqrt{\mu/mc^2}$

cal QPT in the bulk can be also seen for vortices in relativistic superconductors [77].

8.2. Andreev–Majorana bound states on B-phase vortices with broken symmetry

The spectrum in Fig. 15a is valid only for a vortex state that respects all the possible symmetries of the vortex core. These symmetries are the spatial parity P and the discrete symmetry TU_2. The latter is the symmetry under the time reversal T when it is accompanied by the π-rotation U_2 about the axis perpendicular to the vortex axis. In the cores of the experimentally observed vortices in ^{3}He-B, both discrete symmetries are spontaneously broken, while the combined symmetry PTU_2 is preserved [75]. Such a vortex is called the v-vortex. The broken parity in the v-vortex leads to mixing between the two spin components in the core, and as a result, the two AM modes at $p_z = 0$ split. This leads to the spectrum in Fig. 16 [78].

In the weak-coupling regime $mc^2 \ll \mu$, a large number (of the order of $\sqrt{\mu/mc^2}$) of branches appear that cross the zero energy. Each crossing point corresponds to a one-dimensional Fermi surface. This demonstrates that the topology in the bulk determines the spectrum of the fermion zero modes on the B-phase vortices only if the symmetry of the vortex core is not violated. This is a consequence of the mod 2 rule for Majorana modes: a topological zero-energy state survives symmetry breaking only in the case of an odd number of Majorana modes. Hence, for realistic vortices, the AM mode can exist only in half-quantum vortices. For other vortices, such as those in ^{3}He-B, a large number of energy levels is involved. That is why it is more appropriate to use the quasiclassical approximation in the analysis. It leads to other types of topological invariants describing fermion zero modes on vortices (see, e. g., Refs. [9, 79]).

9. CONCLUSION

We considered the AM bound states with zero energy on surfaces, interfaces, and vortices in different phases of p-wave superfluids: ^{3}He-A, ^{3}He-B, planar and polar phases.

These states are determined by topology in the bulk, and they disappear at the QPT from the topological to nontopological state of the superfluid (see the example in Fig. 15). This topology demonstrates the interplay of dimensions. In particular, the 0D Weyl point (the Berry-phase monopole in momentum space) gives rise to a 1D Fermi arc on the surface (Sec. 6.1). The 1D nodal line in the bulk produces the dispersional 2D band of AM modes on the surface (Sec. 5).

The interplay of dimensions also connects the AM states in superfluids in different dimensions. For example, the properties of the spectrum of bound states in the 3D ^{3}He-B are connected to the properties of the spectrum in the 2D planar phase (see Sec. 3 for edge states and Sec. 7.1 for bound states on vortices). The 0D AM mode on a point vortex in a 2D chiral superfluid (Sec. 6) gives rise to a 1D flat band of AM modes on a vortex in the 3D chiral superfluid (Sec. 7).

The most robust zero-energy edge states occur on the boundary of ^{3}He-A, or in general on boundaries and interfaces of chiral superfluids with the topological invariant N in Eq. (1). In other phases, the existence of zero-energy edge states is supported by symmetry, i. e., by the symmetry-protected topological invariants N_K in Eqs. (6) and (17). When the symmetry is violated in the bulk or on the boundary/interface, the AM bound states acquire a gap.

Concerning the AM states on vortices, only the states on half-quantum vortices are fully robust to perturbations. In singly quantized vortices, the fate of zero-energy states depends on symmetry and its possible violation in the bulk or spontaneous breaking inside the vortex core. This is a consequence of the $\mathbb{Z}_2$ classification of AM modes on vortices. On the other hand, the spontaneously broken symmetry inside the vortex core may give rise to many nontopological branches of AM bound states, which cross the zero energy as a function of p_z. This is demonstrated in Sec. 8.2.

We also mention the application to relativistic theories. The fermion zero modes obtained in the Dirac systems, such as the modes localized on strings in Ref. [80], are not properly supported by topology. The reason for that is that the Dirac vacuum is marginal, and the topological invariants depend on the regularization of the Green's function in the ultraviolet [81]. For example, in Fig. 4, the Dirac vacuum is on the border between the trivial vacuum with $N_K = 0$ and the topological vacuum with $N_K = 2$. That is why the existence of the modes with exactly zero energy depends on the behavior of the Green's function at infinity.

The authors acknowledge financial support by the Academy of Finland through its LTQ CoE grant (project No. 250280).

REFERENCES

1. C. W. J. Beenakker, Phys. Rev. Lett. **112**, 070604 (2014).
2. C. Chamon, R. Jackiw, Y. Nishida et al., Phys. Rev. B **81**, 224515 (2010).
3. T. Senthil and M. P. A. Fisher, Phys. Rev. B **61**, 9690 (2000).
4. G. E. Volovik and M. A. Zubkov, Nucl. Phys. B **881**, 514 (2014); arXiv:1402.5700.
5. A. P. Schnyder, S. Ryu, A. Furusaki, and A. W. W. Ludwig, Phys. Rev. B **78**, 195125 (2008).
6. A. P. Schnyder, S. Ryu, A. Furusaki, and A. W. W. Ludwig, AIP Conf. Proc. **1134**, 10 (2009); arXiv:0905.2029.
7. A. P. Schnyder, S. Ryu, and A. W. W. Ludwig, Phys. Rev. Lett. **102**, 196804 (2009); arXiv:0901.1343.
8. A. Kitaev, AIP Conf. Proc. **1134**, 22 (2009); arXiv: 0901.2686.
9. G. E. Volovik, *The Universe in a Helium Droplet*, Clarendon Press, Oxford (2003).
10. G. E. Volovik, Lecture Notes in Phys. **718**, 31 (2007); arXiv:cond-mat/0601372.
11. P. Hořava, Phys. Rev. Lett. **95**, 016405 (2005).
12. M. Z. Hasan and C. L. Kane, Rev. Mod. Phys. **82**, 3045 (2010).
13. Xiao-Liang Qi and Shou-Cheng Zhang, Rev. Mod. Phys. **83**, 1057 (2011).
14. M. A. Silaev and G. E. Volovik, J. Low Temp. Phys. **161**, 460 (2010); arXiv:1005.4672.
15. G. E. Volovik, Pis'ma v Zh. Eksp. Teor. Fiz. **66**, 492 (1997); arXiv:cond-mat/9709084.
16. Suk Bum Chung and Shou-Cheng Zhang, Phys. Rev. Lett. **103**, 235301 (2009); arXiv:0907.4394.
17. G. E. Volovik, Pis'ma v Zh. Eksp. Teor. Fiz. **90**, 440 (2009); arXiv:0907.5389.
18. Y. Nagato, S. Higashitani, and K. Nagai, J. Phys. Soc. Jpn. **78**, 123603 (2009).
19. M. M. Salomaa and G. E. Volovik, Phys. Rev. B **37**, 9298 (1988).

20. G. E. Volovik, Pis'ma v Zh. Eksp. Teor. Fiz. **90**, 639 (2009); arXiv:0909.3084.

21. F. Wilczek, New J. Phys. **16**, 082003 (2014).

22. D. A. Ivanov, Phys. Rev. Lett. **86**, 268 (2001).

23. G. E. Volovik, Pis'ma v Zh. Eksp. Teor. Fiz. **70**, 601 (1999); arXiv:cond-mat/9909426.

24. Y. Tsutsumi, M. Ichioka, and K. Machida, Phys. Rev. B **83**, 094510 (2011).

25. Xiangang Wan, A. M. Turner, A. Vishwanath, and S. Y. Savrasov, Phys. Rev. B **83**, 205101 (2011).

26. A. A. Burkov and L. Balents, Phys. Rev. Lett. **107**, 127205 (2011).

27. M. A. Silaev and G. E. Volovik, Phys. Rev. B **86**, 214511 (2012); arXiv:1209.3368.

28. N. B. Kopnin and M. M. Salomaa, Phys. Rev. B **44**, 9667 (1991).

29. Y. Tanaka and S. Kashiwaya, Phys. Rev. Lett. **74**, 3451 (1995).

30. S. Ryu and Y. Hatsugai, Phys. Rev. Lett. **89**, 077002 (2002).

31. A. P. Schnyder and S. Ryu, Phys. Rev. B **84**, 060504(R) (2011); arXiv:1011.1438.

32. T. T. Heikkilä and G. E. Volovik, Pis'ma v Zh. Eksp. Teor. Fiz. **93**, 63 (2011); arXiv:1011.4185.

33. T. T. Heikkilä, N. B. Kopnin, and G. E. Volovik, Pis'ma v Zh. Eksp. Teor. Fiz. **94**, 252 (2011); arXiv:1012.0905.

34. G. E. Volovik, Pis'ma v Zh. Eksp. Teor. Fiz. **93**, 69 (2011); arXiv:1011.4665.

35. M. Sato, Y. Tanaka, K. Yada, and T. Yokoyama, Phys. Rev. B **83**, 224511 (2011).

36. L. V. Levitin, R. G. Bennett, A. Casey et al., J. Low Temp. Phys. **175**, 667 (2014).

37. H. So, Progr. Theor. Phys. **74**, 585 (1985).

38. K. Ishikawa and T. Matsuyama, Z. Phys. C **33**, 41 (1986).

39. K. Ishikawa and T. Matsuyama, Nucl. Phys. B **280**, 523 (1987).

40. G. E. Volovik, Zh. Eksp. Teor. Fiz. **94**(3), 123 (1988).

41. G. E. Volovik and V. M. Yakovenko, J. Phys.: Condens. Matter **1**, 5263 (1989).

42. D. J. Thouless, M. Kohmoto, M. P. Nightingale, and M. den Nijs, Phys. Rev. Lett. **49**, 405 (1982).

43. Q. Niu, D. J. Thouless, and Y.-Sh. Wu, Phys. Rev. B **31**, 3372 (1985).

44. G. E. Volovik, Pis'ma v Zh. Eksp. Teor. Fiz. **55**, 363 (1992).

45. D. Vollhardt and P. Woelfe, *The Superfluid Phases of Helium 3*, Taylor & Francis (1990).

46. L. Levitin, R. Bennett, A. Casey et al., J. Low Temp. Phys. **158**, 163 (2010).

47. L. V. Levitin, R. G. Bennett, A. Casey et al., J. Low Temp. Phys. **158**, 159 (2010).

48. L. Levitin, R. Bennett, A. Casey et al., Science **340**, 841 (2013).

49. L. V. Levitin, R. G. Bennett, E. V. Surovtsev et al., Phys. Rev. Lett. **111**, 235304 (2013).

50. G. E. Volovik, *Exotic Properties of Superfluid* ^{3}He, World Sci., Singapore (1992).

51. G. E. Volovik, AIP Conf. Proc. **194**, 136 (1989).

52. J. A. Sauls, Phys. Rev. B **84**, 214509 (2011).

53. H. Wu and J. A. Sauls, Phys. Rev. B **88**, 184506 (2013).

54. B. A. Volkov, A. A. Gorbatsevich, Yu. V. Kopaev, and V. V. Tugushev, Zh. Eksp. Teor. Fiz. **81**, 729 (1981); B. A. Volkov and O. A. Pankratov, Pis'ma v Zh. Eksp. Teor. Fiz. **42**, 145 (1985).

55. K. Nagai, Y. Nagato, M. Yamamoto, and S. Higashitani, J. Phys. Soc. Jpn. **77**, 111003 (2008).

56. S. Murakawa, Y. Tamura, Y. Wada et al., Phys. Rev. Lett. **103**, 155301 (2009).

57. J. P. Davis, J. Pollanen, H. Choi et al., Phys. Rev. Lett. **101**, 085301 (2008).

58. Y. Aoki, Y. Wada, M. Saitoh et al., Phys. Rev. Lett. **95**, 075301 (2005).

59. H. Choi, J. P. Davis, J. Pollanen, and W. P. Halperin, Phys. Rev. Lett. **96**, 125301 (2006).

60. Y. M. Bunkov, J. Low Temp. Phys. **175**, 385 (2014).

61. Yu. Makhlin, M. Silaev, and G. E. Volovik, Phys. Rev. B **89**, 174502 (2014); arXiv:1312.2677.

62. M. A. Silaev and G. E. Volovik, Pis'ma v Zh. Eksp. Teor. Fiz. **95**, 29 (2012).

63. V. Gurarie, Phys. Rev. B **83**, 085426 (2011).

64. A. M. Essin and V. Gurarie, Phys. Rev. B **84**, 125132 (2011).

65. L. Fidkowski and A. Kitaev, Phys. Rev. B **81**, 134509 (2010); **83**, 075103 (2011).

66. T. Mizushima, M. Sato, and K. Machida, Phys. Rev. Lett. **109**, 165301 (2012).

67. T. Mizushima, Phys. Rev. B **86**, 094518 (2012).

68. G. E. Volovik, Pis'ma v Zh. Eksp. Teor. Fiz. **91**, 215 (2010).

69. T.-L. Ho, J. R. Fulco, J. R. Schrieffer, and F. Wilczek, Phys. Rev. Lett. **52**, 1524 (1984).

70. M. M. Salomaa and G. E. Volovik, J. Low Temp. Phys. **74**, 319 (1989).

71. M. Nakahara, J. Phys. C **19**, L195 (1986).

72. C. Caroli, P. G. de Gennes, and J. Matricon, Phys. Lett. **9**, 307 (1964).

73. N. Read and D. Green, Phys. Rev. B **61**, 10267 (2000).

74. M. Sato, A. Yamakage, and T. Mizushima, Physica E **55**, 20 (2014).

75. M. M. Salomaa and G. E. Volovik, Rev. Mod. Phys. **59**, 533 (1987).

76. T. Sh. Misirpashaev and G. E. Volovik, Physica B **210**, 338 (1995).

77. Y. Nishida, Phys. Rev. D **81**, 074004 (2010).

78. M. A. Silaev, Pis'ma v Zh. Eksp. Teor. Fiz. **90**, 433 (2009).

79. G. E. Volovik, J. Phys.: Condens. Matter **3**, 357 (1991).

80. R. Jackiw and P. Rossi, Nucl. Phys. B **190**, 681 (1981).

81. G. E. Volovik, Pis'ma v Zh. Eksp. Teor. Fiz. **91**, 55 (2010); arXiv:0912.0502.